Sensing Performance of Multi-Channel RFID-Based Finger Augmentation Devices for Tactile Internet

Federica Naccarata, *Graduate Student Member, IEEE*, Giulio Maria Bianco, *Member, IEEE*, and Gaetano Marrocco, *Senior Member, IEEE*

Abstract—Radiofrequency finger augmentation devices (R-FADs) are a recently introduced class of epidermal radiofrequency identification (RFID) sensor-tags attached to the fingers, communicating with a body-worn reader. These devices are promising candidates to enable Tactile Internet (TI) applications in the short term. R-FAD based on auto-tuning RFID microchips can be used as dielectric probes for the material of touched objects. However, due to the nearly unpredictable intrinsic variability of finger-object interaction, a single sensorized finger (single-channel device) is not enough to guarantee reliable data sampling. These limitations can be overcome by exploiting a multi-channel R-FAD sensorizing multiple fingers of the hand. In this paper, the dielectric-sensing performance of a multi-channel R-FAD, composed of sensors encapsulated into soft elastomers, is numerically and experimentally characterized, involving a set of volunteers. The inter-sensor coupling is negligible, thus enabling simultaneous independent dielectric measurements. The multi-sensor configuration allows for 100% reliability of the on-hand communication link for touched objects in a wide range of permittivity. Experiments moreover demonstrate that multi-channel measurements can halve the measurement uncertainty of the single-channel case. The achievable precision is suitable to discriminate among low-, medium-, and high-permittivity materials.

Index Terms—Auto-tuning antennas, body-area Internet of Things, epidermal sensors, flexible electronic, radiofrequency identification.

I. INTRODUCTION

FINGER augmentation devices (FADs) are finger-worn electronic tools conceived to provide supplemental capabilities through an additional augmentation other than their form [1]. FADs can have different form factors, spanning from proximal-phalanx rings [2] to nail-pads [3], [4], and several possible applications, like driving vehicles [5], [6] or controlling aerial drones [7]. The most ambitious goal of FADs is the achievement of a sensorial*ultrability*, namely providing the user with an artificial sensation to either restore a lost or
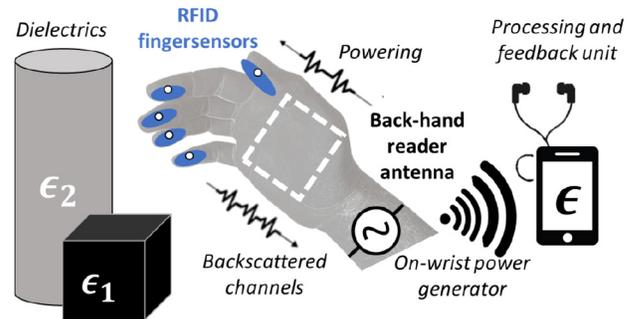

Fig. 1. Pictorial concept of a dielectric sensing multi-channel R-FAD.

degraded natural ability or even to add a new sense, going beyond the natural physical feelings of humans [8].

FADs based on radiofrequency identification (RFID) were proposed to help visually impaired people or to query tagged items [9]–[12]. Tighter integration with flexible sensors directly attached over the fingers' skin denoted as R-FADs (radiofrequency finger augmentation devices), have been introduced in [13]–[16]. R-FADs comprise thin fingertip sensor-tags (hereafter fingertip sensors) that are interrogated by a hand-worn antenna in the 860-960 MHz band (RFID-UHF) driven by a body-worn portable RFID reader. The feedback to the user can be generated by a wireless companion device, like a smartphone, a smartwatch, or earphones (Fig. 1). Numerical investigations [13] demonstrated the system is fully compliant with electromagnetic exposure limits.

A temperature-sensing R-FAD was initially exploited in [14] to restore the physical, thermal feeling lost because of life-saving medical treatments and to investigate cognitive remapping of deafferented patients. Furthermore, the R-FADs are also promising enablers for the Tactile Internet [17], even though current UHF devices still lack high data-rate low latency. Very recently [16], [18], [19], dielectric sensing R-FADs exploited the automatic variation of the impedance of the fingertip sensor's IC (integrated circuit) to sense the dielectric constant of the touched material. This architecture has a potential medical application as an assistive tool for visually impaired people since the provided feedback can help them recognize the material of the object they are handling or touching [16]. A reliable permittivity-sensing R-FAD could be useful also for permittivity-based industrial processes like in the food industry [20] and in agriculture [21], [22].

The practical possibility to collect well separable data when touching the different materials is the rationale to apply a classification procedure for the recognition of the touched object. Preliminary tests evidenced that reader-finger communication can be critical due to the unpredictable modality of finger-object interaction, such as the touch pressure and the inter-user variability [19]. Indeed, the specific morphology of the hand and the grasping gesture is such that the measured data can be highly dependent on the specific sensorized finger. Hence, single-channel measurements are not reliable. Instead, providing the hand with multiple fingertip sensors could enable more degrees of freedom, and it is ultimately expected to improve the reliability of the R-FAD, i.e., the capability of the device to collect data and discriminate the dielectric constant in real use [23]. By expanding the preliminary work in [24], the aim of this paper is twofold, *i)* quantifying the precision of the R-FAD antenna as a dielectric sensor versus the variability of human-object interaction (both the touch-pressure and the individual hand size and grasp modality) and *ii)* investigating how such variability of the measurement can be reduced by resorting to a multi-channel configuration, wherein each finger of the hand can be in principle independently sensorized. The information redundancy is expected to improve the reliability of the link and to get rid of missing readings. Experiments are carried out by using the fingertip antenna from [16], which has been now encapsulated into soft elastomers to make it stretchable and more comfortable for the user.

The paper is organized as follows. The rationale of the dielectric sensing mechanism and metrics are introduced in Section II. Section III describes the electromagnetic characterization of the multi-channel R-FAD, including impedance matching, inter-sensors coupling, and the minimum power the reader has to emit to have the fingertip tag responding. Then, Section IV presents the measurement procedure to determine the performance of the R-FAD as a dielectric sensor in terms of the minimum number of collected samples needed and the effect of touch pressure and of the object's shape. Finally, the reliability of the R-FAD response against the human variability is discussed in Section V with the help of ten volunteers, and the achievable improvement with the multi-channel approach is evaluated.

II. RATIONALE OF DIELECTRIC SENSING AND RELATED METRICS

A. Dielectric Sensing by Auto-Tuning RFID ICs

Dielectric sensing by R-FADs is achieved by exploiting the unique feature of auto-tuning ICs, that can modify their internal radiofrequency impedance to compensate for possible mismatching with the antenna and to maximize the power that the harvesting antenna delivers to the IC itself. Auto-tuning ICs can return a digital metric, denoted as sensor code (s), which is an integer number that is proportional to the retuning effort [25]. The equivalent circuit of the microchip can be modeled as a resistor in parallel with a ladder of capacitors with overall capacitance C_{IC} spanning from a minimum C_{min} to a maximum value with incremental step C_S so that

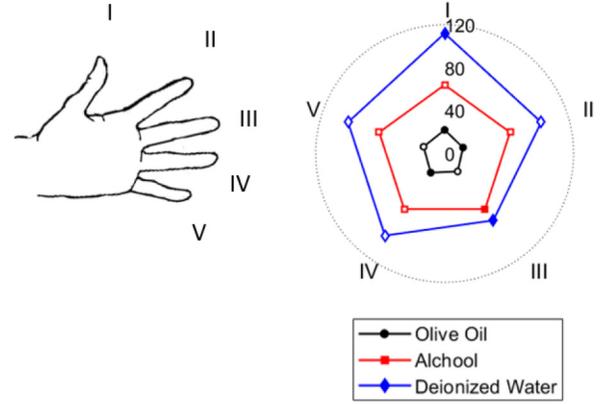$$C_{IC}(s) = C_{min} + sC_S. \tag{1}$$

Fig. 2. Kiavat diagram visualization of digital fingerprints corresponding to three touched dielectric materials. The unfilled markers indicate non-read sensors.

The overall variable susceptance of the IC is derived by the auto-tuning condition [25]

$$|B_{IC}(s) + B_A(\epsilon)| = 0 \tag{2}$$

where $B_{IC}(s) = 2\pi f C_{IC}(s)$ and $B_A(\epsilon)$ are the susceptances of the IC and the antenna, respectively, ϵ is the dielectric constant of the touched object, and f is the frequency.

Equations (1) and (2) hold in a linear range $S_{min} \leq s \leq S_{max}$, outside which saturation occurs [18]. In the linear range, the index s can be related to the antenna input parameters by inverting (2) and accounting for the saturation [26]

$$s(\epsilon) = \text{nint}\left\{-\frac{1}{C_S}\left[C_{IC}(S_{min}) + \frac{B_A(\epsilon)}{2\pi f}\right]\right\}. \tag{3}$$

Possible baselines caused by the specific manufacturing of the fingertip sensor can be removed by employing a *differential sensor code* (Δs) [19]

$$\Delta s(\epsilon) = s(1) - s(\epsilon) \tag{4}$$

where $s(1)$ is the calibration value obtained when the hand is not touching anything ($\epsilon = 1$).

B. Sensing R-FAD Metrics

The information provided by a multi-channel R-FAD is hereafter exploited by introducing the following sensing metrics: the *digital fingerprint* and the *averaged fingerprint*.

1) Digital Fingerprint: Multi-channel R-FADs comprise $1 < N \leq 5$ fingertip sensors. When the wearer touches a dielectric material of permittivity ϵ_m, N sensor codes $\{s_n(\epsilon_m)\}_{n=1,\ldots,N}$ are returned, and the set of differential sensor codes $\{\Delta s_n(\epsilon_m)\}_{n=1,\ldots,N}$ composes the digital fingerprint

$$\mathbf{F}(\epsilon_m) = \{\Delta s_1(\epsilon_m), \ldots, \Delta s_N(\epsilon_m)\}. \tag{5}$$

The N-dimensional fingerprint can be visualized through Kiviat diagrams (Fig. 2). If the kth sensor is not read by the reader in the specific condition, its differential sensor code Δs_k is replaced by the mean over the other responsive fingertip sensors so that its differential sensor code is computed as

$$\Delta s_k(\epsilon_m) = \frac{1}{N_n} \sum_{i=1}^{N_n} \Delta s_i(\epsilon_m), \tag{6}$$
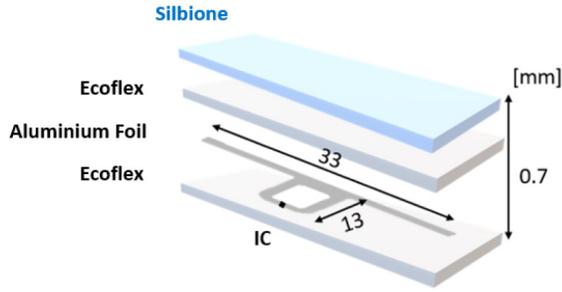
Fig. 3. Exploded view of the fingertip sensor comprising a flexible antenna over curved PET and encapsulating elastomers for comfortable application on the finger.

Fig. 4. Final prototypes of fingertip sensor: (a) stretching, (b) application on a fingertip, and (c) finger bending.

TABLE I
ELECTRICAL CHARACTERISTICS OF THE EMPLOYED
MATERIALS (f = 867 MHz)

Material	σ [S/m]	ϵ
Ecoflex^{TM} 00-30	$\sigma = 0.007$	2.7
Silbione^{TM}	$\sigma = 0.012$	2.5
Closed-cell PVC foam [27]	$\sigma = 2.2 \cdot 10^{-5}$	2.3
Homogeneous body tissue [13]	$\sigma = 0.62$	30
Olive oil [19]	$\sigma = 0.026$	3
Ethyl alcohol (90%) [28]	$\sigma = 10^{-5}$	17
Deionized water [29]	$\sigma = 0.05$	78

where N_n is the number of responsive fingertip sensors.

2) Averaged Fingerprint: The mean of the differential sensor codes of all sensors of the hand gives the averaged fingerprint

$$\overline{F}(\epsilon_m) = \frac{1}{5} \sum_{i=1}^{5} \Delta s_i(\epsilon_m). \tag{7}$$

III. THE MULTI-CHANNEL R-FAD

The layout of the reference finger antenna to evaluate the above-defined metrics is derived from [16]. It is a T-matched aluminum dipole soldered to Axzon Magnus-S3 ICs having input admittance $G_{IC} = 0.482$ mS and equivalent capacitance derived from (1) with parameters $C_{min} = 1.9$ pF, $C_S = 3.1$ fF, $\{S_{min}, S_{max}\} = \{80, 400\}$.

The dipole is encapsulated between two layers of Ecoflex^{TM} 00-30 (by Smooth-On; thickness $\sim$ 0.3 mm each) silicone, which are cured together with a layer of Silbione^{TM} (by Elkem Silicones; thickness $\sim$ 0.1 mm; Fig. 3). The Ecoflex^{TM} acts as a coating film for the sensor, whereas the Silbione^{TM} ensures adherence to the finger's skin. The electrical properties of the two silicone rubbers, as measured with a two-port ring resonator [30], are listed in Table I. The resulting fingertip sensors are highly flexible, stretchable, biocompatible, and can be removed and re-applied comfortably (Fig. 4). They also withstand disinfection by hydrogen peroxide. The reader antenna is a folded patch on a closed-cell PVC (polyvinyl chloride) foam as in [13] that is placed on the back of the hand.

A. Impedance Matching

The fingertip sensor is numerically simulated[1] when it is placed on a homogeneous phantom of the hand (from [18]).

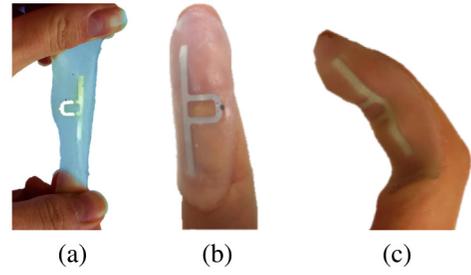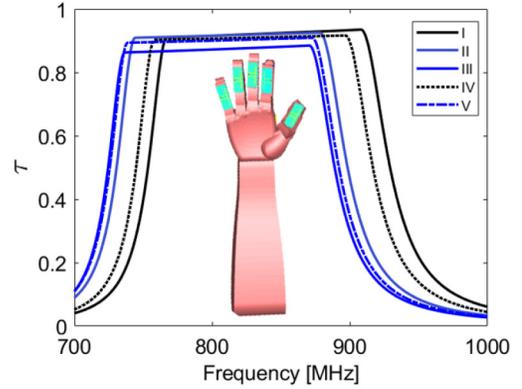[1] Numerical simulations by CST - Microwave Studio 2018.

Fig. 5. The simulated power transmission coefficient of each fingertip sensor. In the inset: the simplified homogeneous model of the hand from [18].

Fig. 5 shows the power transfer coefficients $\tau(f)$, which is the fraction of the RF power that is harvested by the antenna and then transferred to the IC. The power transfer coefficient is computed by accounting for the auto-tuning according to (2) as in [16],

$$\tau(f) = \begin{cases} \frac{4G_{IC}G_A}{|G_{IC}+G_A+j(B_A+2\pi f C_{min})|^2} \\ \quad \text{if } B_A > -2\pi f C_{min} \\ \frac{4G_{IC}G_A}{(G_{IC}+G_A)^2} \\ \quad \text{elsewhere} \\ \frac{4G_{IC}G_A}{|G_{IC}+G_A+j[B_A+2\pi f(C_{min}+sC_S)]|^2} \\ \quad \text{if } B_A < -2\pi f(C_{min} + S_{max}C_S) \end{cases} \tag{8}$$

where G_A is the conductance seen by the IC. Thanks to the auto-tune property of the IC, τ exhibits the typical nearly flat profile over broadband. The power transfer coefficient at the EU RFID frequency is $\tau(867 \text{ MHz}) > 0.85$ for any fingertip sensor.

B. Inter-Antenna Coupling

The electromagnetic coupling among fingertip antennas when all the fingers are sensorized is here evaluated. Coupling is relevant to the cross-sensitivity of multiple sensors on the same hand, namely the possible dependence of the response of any considered fingertip sensor on the others.

The electric near field is computed over the fingers when each antenna is singularly excited while the others are not. The color map in Fig. 6 shows that, by the naturally decoupling effect of the human tissue absorption, the strength of the
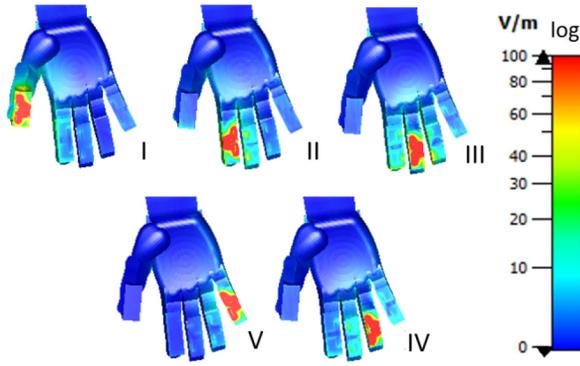
Fig. 6. Numerical simulations of the inter-sensor electromagnetic coupling of the multi-channel R-FAD. Map of the E-field when only one of the five ports is sourced by 1 W power. Roman numerals identify the finger of the active antenna.
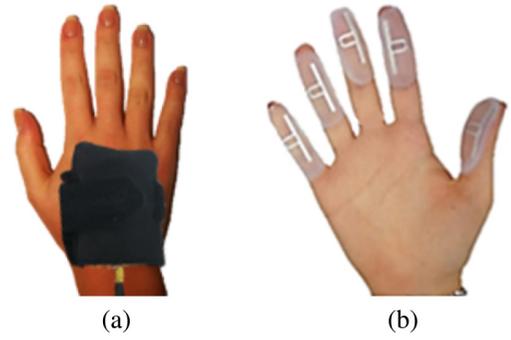

Fig. 7. (a) Back-hand reader antenna. (b) The five fingertip sensors worn simultaneously.
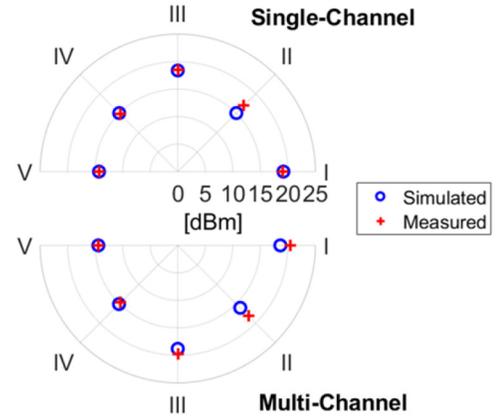

Fig. 8. Simulated and measured turn-on powers (at $f = 867$ MHz) in the case of the single-channel (only a sensorized fingertip at a time) and the multi-channel (all fingers simultaneously sensorized) on-body link.

fields on non-excited fingertip sensors is less than 10% that of the excited one. The coupling can be quantified through Kurokawa's generalized scattering matrix $\mathbf{K}$ accounting for the ICs complex impedances [31], [32]

$$\mathbf{K} = \mathbf{G}(\mathbf{Z} - \mathbf{H}^+)(\mathbf{Z} + \mathbf{H})^{-1}\mathbf{G}^{-1}. \quad (9)$$

$\mathbf{Z}$ is the antennas' impedance matrix, "$+$" indicates the complex conjugate transpose matrix, and $\mathbf{G}$ and $\mathbf{H}$ are diagonal matrices whose non-null components are equal to $0.5[\text{Re}(Z_C)]^{-0.5}$ and Z_C, respectively. Z_C is the complex impedance of the ICs assumed fixed in the middle range ($Z_C = (2.8 - j76)\,\Omega$ [26]). The normalized scattering matrix of the fingertip sensors' ports at $f = 867$ MHz is

$$\frac{\left|\mathbf{K}_{jk}\right|}{\max\limits_{j,k}\left[\left|\mathbf{K}_{jk}\right|\right]} = \frac{1}{100}\begin{bmatrix} \mathbf{98.74} & 0.15 & 0.09 & 0.04 & 0.01 \\ 0.15 & \mathbf{88.71} & 2.89 & 0.43 & 0.05 \\ 0.09 & 2.89 & \mathbf{91.38} & 0.86 & 0.01 \\ 0.04 & 0.43 & 0.86 & \mathbf{97} & 0.08 \\ 0.01 & 0.05 & 0.53 & 0.08 & \mathbf{100} \end{bmatrix}. \quad (10)$$

The inter-sensor coupling is rather modest since the off-diagonal elements are $\lesssim 3\%$ of the diagonal ones. Further numerical simulations assessed that there is no significant change in the electromagnetic coupling even when the fingers are bent during the grasping gesture. Accordingly, the six-port multi-channel R-FAD can be reduced to five two-port models, one for each reader-tag link [18].

Therefore the mutual hand-finger links are mostly unaffected by the simultaneous wearing of multiple sensors and, consequently, the cross-sensitivity of the sensors is negligible.

C. Electromagnetic Performance

The electromagnetic performance of the prototypes is characterized by the Voyantic Tagformance Pro station. The reader antenna is positioned on the back of the hand (Fig. 7(a)), and it is moderately conformable to the user's hand morphology. The measurements are made by asking a volunteer to first wear just one sensor at a time on each finger (single-channel) and then all the five sensors (multi-channel; Fig. 7(b)) with the hand straight open without touching anything. The orientation of the fingertip sensors was experimentally determined to minimize the body shadowing caused by the nearby fingers.

In all cases, the Tagformance raises the emitted power until the kth fingertip sensor starts responding, and that threshold value is the *turn-on power* of that fingertip antenna in the current condition. The turn-on power was predicted by means of the transducer power gain and the IC sensitivity [18] and is the considered communication performance metric.

As expected by the previous numerical analysis, the recorded turn-on powers confirm no significant difference in the case of single-sensor and multi-sensors configurations (Fig. 8) since the antennas are negligibly coupled. All the fingertip sensors require the generator to feed the reader antenna with less than 25 dBm, compatible with hand-held readers having a size similar to watches or key-fobs. For this input power, numerical simulations (not reported here) returned a maximum SAR (Specific Absorption Rate) in the hand of about 2 W/kg in the most conservative case of continuous emission. This value is fully compliant with the exposure limit (4 W/kg) [33].

IV. Performance as Dielectric Tactile Sensor

This Section introduces the experimental set-up and the processing to evaluate the performance of the R-FAD as a dielectric sensor according to the metrics introduced in Section II. In particular, this Section discusses the minimum number of sensor code samples that guarantees a reliable

(a)

(b)

Fig. 10. (a) Continuous acquisition of the sensor code *s* while the bare sensor (not attached to the finger) is in the air and when it adheres to a bottle filled with a given liquid. (b) Amplitude spectrum of $s(t)$ evaluated through Fast Fourier Transform (FFT).

(a)

(b)

(c)

(d)

(e)

(f)

Fig. 11. Convergence error vs the permanent regime over an increasing number of samples when the sensorized finger touches three different materials: olive oil, alcohol, and deionized water. (a,b,c) Convergence error of the average. (d,e,f) Convergence error of the median.
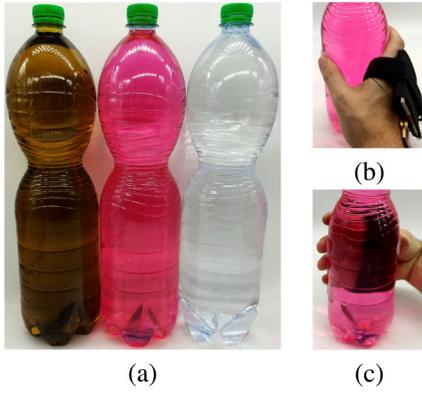

(a)

(c)

Fig. 9. Experimental set-up. (a) Three PET bottles filled with the three dielectric liquids. (b,c) The performed reference grasp gesture to touch the bottles.

measurement outcome, and it investigates the sources of uncertainty posed by the touch pressure variability and different containers of the liquids.

A. Reference Objects

The experimental reference set-up comprises three equal-size PET (polyethylene terephthalate, $\epsilon = 2.5$ [18]) bottles having a diameter 6.5 cm and thickness 0.3 mm. Different containers from the reference one are utilized to assess their impact on sensing in Section IV-D. The containers are filled with three dielectric liquids of common use: olive oil, ethyl alcohol, and deionized water (Fig. 9(a); electric properties in Table I). The liquids have high dielectric contrast, so they are suitable to test the sensors' response in both low-medium and medium-high permittivity ranges. The R-FAD wearer is asked to normally grasp the bottles (Fig. 9(b,c)) and the sensor code is collected.

B. Measurement Time Window

When the sensor contacts an object, the auto-tune functionality of the microchip activates and after an initial transient, it stabilizes, fluctuating around a baseline that depends on the touched material. The fluctuation is the consequence of the charge and discharge of the internal equivalent capacitor during the RFID interrogation. Accordingly, the measurement time window must be large enough to fade the touch transient and then to drop out the fluctuations by averaging. The typical behavior of the fluctuation in the static condition, namely when just the bare sensor was directly attached to the bottle without the presence of the finger, is a sawtooth profile (Fig. 10(a)). Independently from the contacted material, it is characterized by a dominant frequency of 0.7 Hz (Fig. 10(b)). Hence, at least one period (1.4 s) must be sampled to remove fluctuations by averaging.

The duration of the transient when the wearer touches the bottle is estimated through the evaluation of the convergence error δ. The convergence error is used to derive the number of samples needed to obtain stable metrics and is defined as [34]

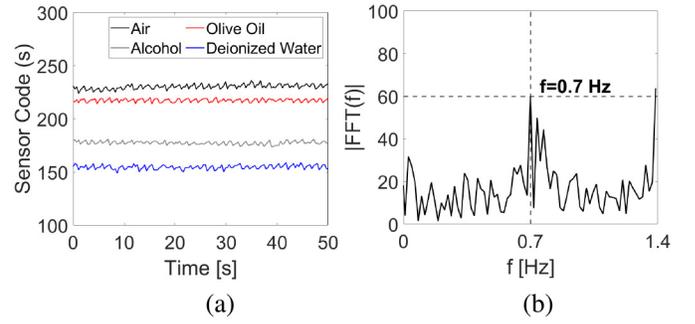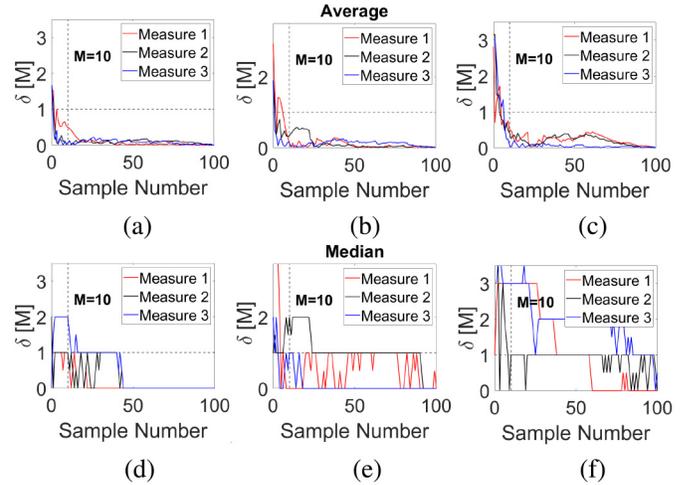$$\delta[M] = \sigma_s[M] - \sigma_s[M_\infty]. \qquad (11)$$

$\sigma_s[M]$ is the standard deviation of the sensor code evaluated on M samples, whereas $\sigma_s[M_\infty]$ approximates the asymptotic value corresponding to $M_\infty = 100$ samples. The minimum number M_0 of samples for averaging to return a stable measurement is determined so that $\delta[M_0] < 1$. This analysis also accounts for the effect of fluctuations. M_0 was evaluated through measurements of the sensor code when the fingertip sensors touched three times each liquid. Fig. 11(a,b,c) shows that M_0 is higher as the material's permittivity increases so that the value $M_0 = 10$ is considered as a valid trade-off for all three materials. Since the sampling period of the RFID reader is 0.7 s, the acquisition time window will be therefore 7 s, which is also suitable to drop out the natural fluctuation of the sensor code, as described above. Another option for data analysis could be the median that is more robust against outliers. However, the time required to have a stable measurement is longer than the mean (Fig. 11(d,e,f)), taking up to 90 samples versus 10 samples for the average to return a convergence error lower than a single unit. Accordingly, the mean operator will be hereafter used. Measurements could be significantly sped up by accepting a convergence error of 2 units instead of 1, so to add one unit of uncertainty. In this case,
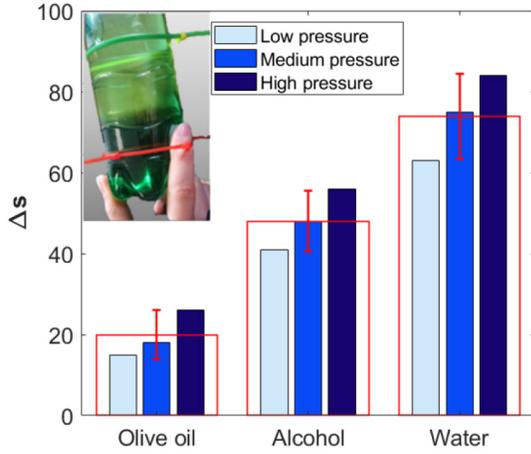
Fig. 12. Measured digital fingerprints corresponding to increasing touch pressures on the bottles filled by the three liquids. The wide red bars indicate the mean values, and the standard deviation σ_p is also represented.
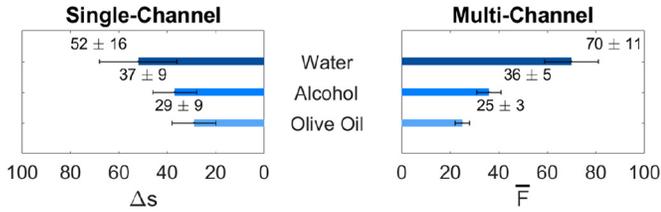

Fig. 13. Comparison between the differential sensor code Δs of the single-channel (fingertip sensor II) and the averaged fingerprint $\overline{F}$ of the multi-channel R-FAD. Black segments indicate uncertainties.

the measurement time could be reduced to just 2 seconds. This choice is still compliant with the possibility to discriminate the considered liquids. To be more conservative, the convergence error lower than 1 unit and the corresponding $M_0 = 10$ are hereafter assumed.

C. Touch Variability

The inter-user and inter-finger variabilities introduce an unpredictable offset for each contacted material, notwithstanding the monotonic behavior of the differential sensor code $\Delta s(\epsilon)$ for a given user and gesture [19]. Namely, touch pressure is expected to modify the effective permittivity sensed by the fingertip antenna. The stronger the pressure, the larger the adhesion and hence the higher the effective permittivity perceived by the fingertip antenna. The precision of the measurement is hence related to the unpredictable touch pressure.

To quantify this effect, the differential sensor code Δs of a fingertip-sensor is measured when the touch pressure is mechanically increased in a controlled way. For this purpose, the index finger (diameter 1 cm) of a volunteer is kept fixed over a bottle (diameter 6.5 cm) by using a plastic tie. Three pressure levels are enforced by fastening the tie according to three perimeters: 8.5 cm for the low-pressure, 8 cm for the medium, and 7.6 cm for the high. The corresponding pressures include the physiological variations and range from the barely-fixed to the tightly-bound finger. The higher the pressure applied, the better the IC adheres to the object, the higher
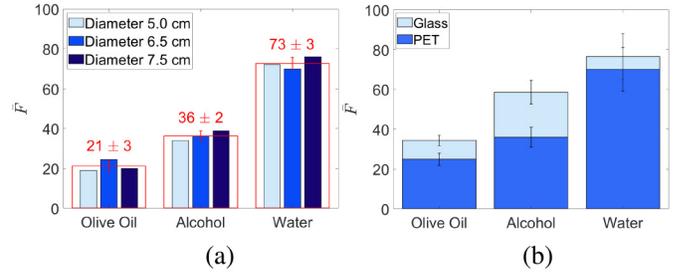

Fig. 14. Averaged fingerprints $\overline{F}$ of the multi-channel R-FAD when (a) touching PET bottles with different diameters and (b) touching bottles glass in comparison with the PET case.
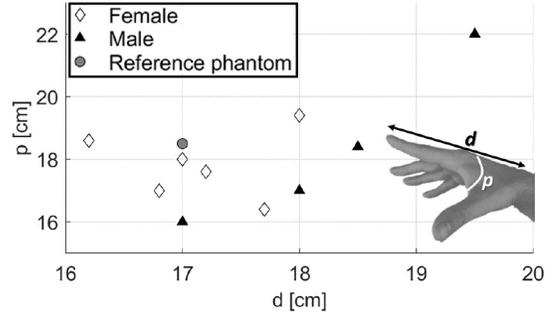

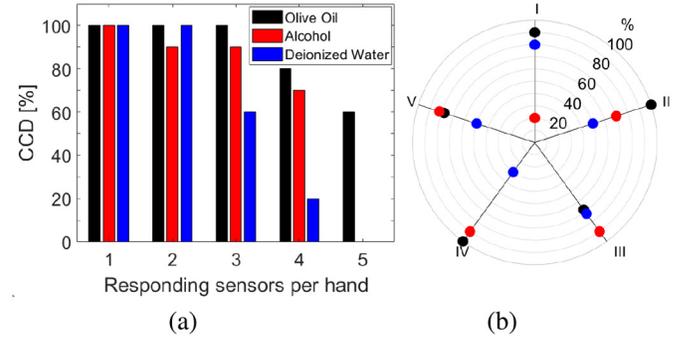Fig. 15. Hand sizes (wrist-fingertip distance d and palm perimeter p) of the ten volunteers.

Fig. 16. (a) Complementary cumulative distribution (CCD) bar of the simultaneously responding finger-sensors of the same hand over the test population. (b) Percentages of the readable sensors per specific finger of the same hand of the volunteers when touching the three objects (color markers as in the inset on the left).

the returned Δs is (Fig. 12). The estimated precision is dependent on the touched object and, in particular, it gets worse along with the increase of the permittivity. However, the relative precision $\sigma_p/\Delta s$ is bounded to $|\sigma_p/\Delta s| < 0.3$ so that a conservative estimate of the precision of any measurement of Δs with uncontrolled touch pressure is $\sigma_p = 0.3\Delta s$. However, it can be improved (i.e., reduced) by evaluating the averaged fingerprint $\overline{F}$ on N_n sensors of the hand's fingertips touching the same material as stated by the propagation of uncertainty formula [35], [36]

$$\overline{\sigma}_F = \sqrt{\frac{\sum_{i=1}^{N} \sigma_{p,i}^2}{N_n^2}} \leq \frac{0.3}{N_n}\sqrt{\sum_{i=1}^{N} \Delta s_i^2}. \quad (12)$$

For instance, Fig. 13 shows the R-FADs digital metric and the corresponding standard deviations that are produced by
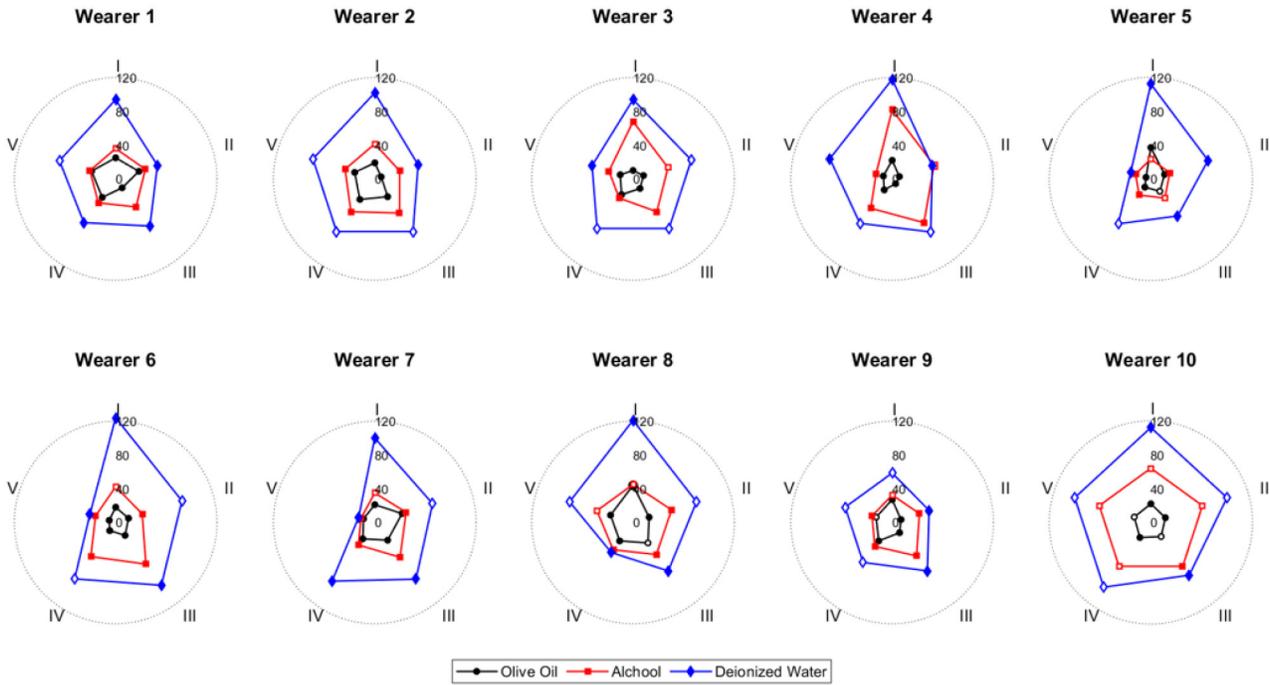
Fig. 17. Digital fingerprints of the test population when the multi-channel R-FADs are naturally touching the three materials with no control on the pressure. The unfilled markers symbolize non-read sensors.

the same volunteer as above without any control on the touch pressure in the case of the only index finger, and then when all the fingers are sensorized. By the effect of (12), the standard deviation is nearly halved in the multi-channel configuration. It is also worth noticing that the effect of the stiffness of the object is comparable to a different pressure applied, and that $\overline{F}$ increases by about 1 unit every 0.6 unit of dielectric contrast.

D. Size and Material of the Container

The variability of the dimension, thickness, and material of the container of the dielectric liquids affects the sensor code returned by the system. For instance, by varying the diameter of the PET bottles of ± 1.25 cm, the uncertainty on the averaged fingerprint is of 3 units (Fig. 14(a)).

A bottle of ordinary glass (diameter 6.5 cm, thickness 1.6 mm, $\epsilon = 6.9$ [37]) is considered to evaluate the sensing capabilities of the R-FAD when using a different container. The glass thickness and permittivity raise all the averaged fingerprints (Fig. 14(b)). Even though the contrast between the alcohol and the deionized water is reduced, it is still possible to distinguish the materials with a remarkable margin.

V. RELIABILITY OF THE R-FAD RESPONSE

The last experimental campaign is aimed at quantifying the reliability of the on-hand link when touching objects and, in particular, the overall variability of the multi-channel R-FAD responses. A test population of ten healthy volunteers having different hand sizes (Fig. 15) is sensorized over all the five fingers of the hand. They are asked to naturally grasp (with no mechanical control on the touch pressure) the three reference PET bottles as above. The experiments are repeated three times for a total of 450 measurements.

A. Statistic of Responding Finger-Sensors

Fig. 16(a) presents the complementary cumulative distribution (CCD) bar of the responding fingers of the same hand so that $CDD(m)$ is the percentage, over the test population, that at least m fingertip sensors of the same hand respond to the reader. Measurements show that at least one finger will provide information in all ($CDD(1) = 100\%$) combinations (user-material). Over all the three materials, at least two fingers provide meaningful data in 90% of the cases and three fingers in 60%. There is no case when all the fingers respond at the same time.

Further insight into the communication can be gained by the polar diagram in Fig. 16(b), showing the percentage of responding finger-sensors with respect to the filling liquid of the bottles. The ideal condition would be all the three color markers concentrated on the 100% circle. No finger would always be responsive for all the materials on the entire population of users. Finger III is, however, the most reliable one, with a probability of 70% of response when touching all three objects. The thumb and the IV finger are the least reliable ones (percentage of 20% and 30%, respectively). Finally, fingers II and V provide intermediate reliability of 50%. Thus, sensors could be just placed on fingers II, III, and V.

B. Digital Fingerprints and Statistics

The digital fingerprints returned by the multi-channel R-FAD system are reported in Fig. 17 for each volunteer. As expected by simulations, the digital fingerprints increase along with the permittivity, and the corresponding polygons enlarge accordingly in most of the considered cases, thus providing the base for automatic classification of the touched materials. In
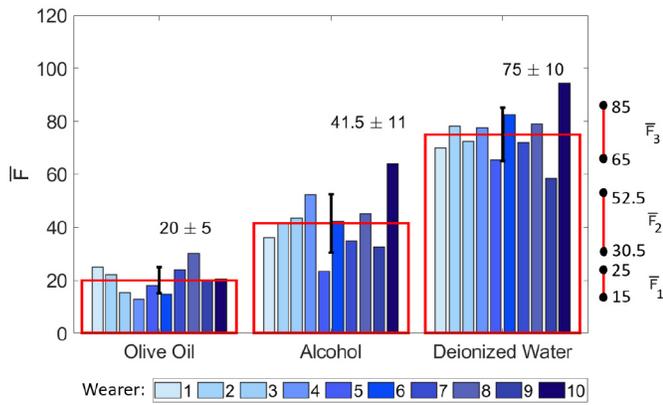
Fig. 18. Averaged fingerprints $\overline{F}$ of the ten volunteers when touching the three objects with increasing permittivity. The macro red bars indicate the average and standard deviation over the population. On the right, the overall span of the $\overline{F} \pm \sigma$ for the three materials.

some cases, up to three finger-sensors do not respond (unfilled markers), but the presence of the other sensors permits to guarantee response reliability at the hand level. The Kiavat diagrams show a large variability among the sensors, that are mostly caused by i) the morphology of the wearer's hand and fingers, ii) the applied pressures, iii) the differences in the grasping gesture like the distance between fingers and tags' orientation, and iv) the eventual fabrication imperfections of the auto-tuning ICs.

The inter-user variability of the averaged fingerprint can be quantified with the help of the bar diagram in Fig. 18, wherein the responses of the populations are grouped by the kind of materials ranked according to their permittivity. The standard deviation is less than 11 units for all three classes and just 5 units in the case of the lowest-permittivity liquid. These values are, however, such to not induce overlapping among adjacent classes; therefore, the materials can be discriminated by just applying thresholds.

VI. CONCLUSION AND FUTURE WORKS

When attached to the five fingers of the hand, the flexible and stretchable fingertip antennas with auto-tuning RF ICs are weakly coupled, thus enabling independent dielectric measurements. A stable RFID link with a back-hand-mounted patch antenna interrogator can be established with less than 25 dBm of emitted power. A reliable measurement of the sensor code metric, which can be related to the touched object's permittivity, requires the calculation of the average on 10 samples to get rid of intrinsic fluctuations and of the transient required by auto-tuning to stabilize. The random touch force introduces a 30% uncertainty in the differential sensor code of the single sensor that can be reduced to one half by resorting to a multi-sensor configuration that also allows for a 100% reliability of the communication with at least one finger in all considered tests over a 10-volunteer set. The precision of the averaged fingerprint measurement is always less than 11 units (over the useful range $80 \leq s \leq 400$), which is suitable to discriminate at least three classes of liquids with low, medium, and high permittivity.

Although the method has been just applied to materials of rather different permittivities, it is reasonably expected that a better resolution could be achieved by the application of machine learning classification exploiting additional information such as the amplitude and phase of the backscattered power returned by the device, as already done in [38]. Such algorithms could also be exploited to recognize different grasping gestures, allowing for sensing even when some fingersensors do not adequately adhere or do not contact the material to be sensed. Another possible future direction of research is the optimization of the fingertip sensors in terms of overall size to simultaneously ensure significative susceptance variations and similar contact areas over the five fingers when grasping dielectric objects.

REFERENCES

[1] R. Shilkrot, J. Huber, J. Steimle, S. Nanayakkara, and P. Maes, "Digital digits: A comprehensive survey of finger augmentation devices," *ACM Comput. Surv.*, vol. 48, no. 2, pp. 1–29, 2015.

[2] M. Wilhelm, D. Krakowczyk, and S. Albayrak, "PeriSense: Ring-based multi-finger gesture interaction utilizing capacitive proximity sensing," *Sensors*, vol. 20, no. 14, pp. 1–23, 2020.

[3] L. Yin et al., "A passive perspiration biofuel cell: High energy return on investment," *Joule*, vol. 5, pp. 1–17, Jul. 2021.

[4] D. Lee, S. Lee, and I. Oakley, "Nailz: Sensing hand input with touch sensitive nails," in *Proc. Conf. Human Factors Comput. Syst.*, 2020, pp. 1–13.

[5] L.-B. Bilius and R.-D. Vatavu, "A multistudy investigation of drivers and passengers' gesture and voice input preferences for in-vehicle interactions," *J. Intell. Transp. Syst. Technol. Plan. Oper.*, vol. 25, no. 2, pp. 197–220, 2020.

[6] B.-F. Gheran and R.-D. Vatavu, "From controls on the steering wheel to controls on the finger: Using smart rings for in-vehicle interactions," in *Proc. ACM Des. Interact. Syst. Conf.*, 2020, pp. 299–304.

[7] Y.-P. Yau, L. Lee, Z. Li, T. Braud, Y.-H. Ho, and P. Hui, "How subtle can it get?: A trimodal study of ring-sized interfaces for one-handed drone control," *Proc. ACM Interact. Mobile Wearable Ubiquitous Technol.*, vol. 4, no. 2, pp. 1–29, 2020.

[8] R. Shilkrot, "Digital digits: Designing assistive finger augmentation devices," Ph.D. dissertation, Dept. Architecture, Massachusetts Inst. Technol., Boston, MA, USA, 2015.

[9] P. Sedighi, M. H. Norouzi, and M. Delrobaei, "An RFID-based Assistive glove to help the visually impaired," *IEEE Trans. Instrum. Meas.*, vol. 70, Mar. 2021, Art. no. 4004109. [Online]. Available: https://ieeexplore.ieee.org/document/9389748

[10] R. K. Singh, A. Michel, P. Nepa, A. Salvatore, M. Terraroli, and P. Perego, "Compact and wearable Yagi-like textile antennas for near-field UHF-RFID readers," *IEEE Trans. Antennas Propag.*, vol. 69, no. 3, pp. 1324–1333, Mar. 2021.

[11] P. S. Taylor and J. C. Batchelor, "Finger-worn UHF far-field RFID tag antenna," *IEEE Antennas Wireless Propag. Lett.*, vol. 18, pp. 2513–2517, 2019.

[12] R.-H. Liang, S.-Y. Yang, and B.-Y. Chen, "IndexMO: Exploring finger-worn RFID motion tracking for activity recognition on tagged objects," in *Proc. Int. Symp. Wearable Comput.*, 2019, pp. 129–134.

[13] S. Amendola, V. Di Cecco, and G. Marrocco, "Numerical and experimental characterization of wrist-fingers communication link for RFID-based finger augmented devices," *IEEE Tran. Antennas Propag.*, vol. 67, no. 1, pp. 531–540, Jan. 2019.

[14] S. Amendola, V. Greco, G. M. Bianco, E. Daprati, and G. Marrocco, "Application of radio-finger augmented devices to cognitive neural remapping," in *Proc. IEEE Int. Conf. RFID Technol. Appl.*, 2019, pp. 258–262.

[15] V. Di Cecco, S. Amendola, P. P. Valentini, and G. Marrocco, "Finger-augmented RFID system to restore peripheral thermal feeling," in *Proc. IEEE Int. Conf. RFID*, 2017, pp. 54–60.

[16] G. M. Bianco and G. Marrocco, "Fingertip self-tuning RFID antennas for the discrimination of dielectric objects," in *Proc. 13th Eur. Conf. Antennas Propag.*, Krakow, Poland, Mar. 2019, pp. 1–4.

[17] V. Fanibhare, N. I. Sarkar, and A. Al-Anbuky, "A survey of the tactile Internet: Design issues and challenges, applications, and future directions," *Electronics*, vol. 10, no. 17, pp. 1–35, 2021.

[18] G. M. Bianco, S. Amendola, and G. Marrocco, "Near-field constrained design for self-tuning UHF-RFID antennas," *IEEE Trans. Antennas Propag.*, vol. 68, no. 10, pp. 6906–6911, Oct. 2020.

[19] G. M. Bianco, C. Vivarelli, S. Amendola, and G. Marrocco, "Experimentation and calibration of near-field UHF epidermal communication for emerging tactile Internet," in *Proc. 5th Int. Conf. Smart Sustain. Technol.*, Split, Croatia, 2020, pp. 1–4.

[20] W. Routray and V. Orsat, "Recent advances in dielectric properties–measurements and importance," *Current Opinion Food Sci.*, vol. 23, pp. 120–126, Oct. 2018.

[21] R. D. Magarey, R. C. Seem, A. Weiss, T. Gillespie, and L. Huber, "Estimating surface wetness on plants," in *Micrometeorology in Agricultural Systems*. Madison, WI, USA: Amer. Soc. Agronomy, 2015, pp. 199–226.

[22] N. D. Kaptein, M. E. Light, and M. J. Savage, "Sensors for the improvement of irrigation efficiency in nurseries," *Water SA*, vol. 45, no. 3, pp. 527–535, Jul. 2019.

[23] T. Aven, "The reliability science: Its foundation and link to risk science and other sciences," *Rel. Eng. Syst. Safety*, vol. 215, pp. 1–7, Nov. 2021.

[24] F. Naccarata, G. M. Bianco, and G. Marrocco, "Multi-channel radiofrequency finger augmentation device for tactile Internet," in *Proc. 34th Gen. Assoc. Sci. Symp. Int. Union Radio Sci.*, Rome, Italy, Aug. 2021, pp. 1–4.

[25] M. C. Caccami and G. Marrocco, "Electromagnetic modeling of self-tuning RFID sensor antennas in linear and nonlinear regimes," *IEEE Trans. Antennas Propag.*, vol. 66, no. 6, pp. 2779–2787, Jun. 2018.

[26] G. M. Bianco and G. Marrocco, "Sensorized facemask with moisture-sensitive RFID antenna," *IEEE Sens. Lett.*, vol. 5, no. 3, pp. 1–4, Mar. 2021.

[27] R. Lodato, V. Lopresto, R. Pinto, and G. Marrocco, "Numerical and experimental characterization of through-the-body UHF-RFID links for passive tags implanted into human limbs," *IEEE Trans. Antennas Propag.*, vol. 62, no. 10, pp. 5298–5306, Oct. 2014.

[28] R. J. Sengwa, "Comparative dielectric study of mono, di and trihydric alcohols," *Indian J. Pure Appl. Phys.*, vol. 41, no. 4, pp. 295–300, Apr. 2003.

[29] C. G. Malmberg and A. A. Maryott, "Dielectric constant of water from 0 to 1000 C," *J. Res. Nat. Bur. Stand.*, vol. 56, no. 1, pp. 1–8, Jan. 1956.

[30] P. A. Bernard and J. M. Gautray, "Measurement of dielectric constant using a microstrip ring resonator," *IEEE Tran. Microw. Theory Techn.*, vol. 39, no. 3, pp. 592–595, Mar. 1991.

[31] P. V. Nikitin, K. V. S. Rao, S. F. Lam, V. Pillai, R. Martinez, and H. Heinrich, "Power reflection coefficient analysis for complex impedances in RFID tag design," *IEEE Trans. Microw. Theory Techn.*, vol. 53, no. 9, pp. 2721–2725, Sep. 2005.

[32] K. Kurokawa, "Power waves and the scattering matrix," *IEEE Trans. Microw. Theory Techn.*, vol. 13, no. 2, pp. 194–202, Mar. 1965.

[33] "On the limitation of exposure of the general public to electromagnetic fields 0 Hz–300 GHz," Commission Eur. Communities, Brussels, Belgium, Rep. 98/0166, 1999. Accessed: Mar. 16, 2022. [Online]. Available: https://www.eumonitor.nl/9353000/1/j4nvke1fm2yd1u0_j9vvik7m1c3gyxp/vkcweea2odz3/v=s7z/f=/com(1998)268_en.pdf

[34] F. Camera and G. Marrocco, "Electromagnetic-based correction of bio-integrated RFID sensors for reliable skin temperature monitoring," *IEEE Sensors J.*, vol. 21, no. 1, pp. 421–429, Jan. 2021.

[35] *Evaluation of Measurement Data–Guide to the Expression of Uncertainty in Measurements*, Standard JCGM 100:2008, Sep. 2008.

[36] S. G. Rabinovich, *Measurement Errors and Uncertainties—Theory and Practice*, 3rd ed. New York, NY, USA: Springer-Verlag, 2005.

[37] M. Ye, B. Wang, and S. Sato, "Effects of dielectric constant of glass substrates on properties of liquid crystal lens," *IEEE Photon. Technol. Lett.*, vol. 19, no. 17, pp. 1295–1297, Sep. 1, 2007.

[38] C. Occhiuzzi *et al.*, "Radio-frequency-identification-based intelligent packaging: Electromagnetic classification of tropical fruit ripening," *IEEE Antennas Propag. Mag.*, vol. 62, no. 5, pp. 64–75, Oct. 2020.

Federica Naccarata (Graduate Student Member, IEEE) was born in Bari in 1996. She received the M.Sc. degree (Hons.) in medical engineering from the University of Rome Tor Vergata, Italy, in 2021, where she is currently pursuing the Ph.D. degree in computer science, control, and geoinformation. Her research interests mainly include RFID systems, wearable antennas for Tactile Internet, implantable antennas, and cyber prostheses.

Giulio Maria Bianco (Member, IEEE) received the M.Sc. degree (Hons.) in medical engineering from the University of Roma Tor Vergata, Italy, in 2018, and the Ph.D. degree (Hons.) in computer science, control, and geoinformation from the University of Roma Tor Vergata in 2022, in collaboration with the European Academy of Bolzano. He is a Postdoctoral Researcher with the Pervasive Electromagnetics Lab and RADIO6ENSE Srl, a spin-off of the Tor Vergata University. His research is focused on wireless devices for body-area IoT systems. He has been a member of the Pontifical Council for Culture Youth Forum since 2019. He won two Young Scientist Awards from URSI in 2020 and 2022 with his work on modeling body-centric wireless communications.

Gaetano Marrocco (Senior Member, IEEE) is a Full Professor with the University of Roma Tor Vergata, where he serves as the Chair of the Medical Engineering School. His research is currently focused on wireless-activated sensors, wearable and epidermal electronics, structural antennas for smart prosthesis, and finger augmentation devices for Tactile Internet. He serves as an Associate Editor for the IEEE JOURNAL OF RADIOFREQUENCY IDENTIFICATION and the IEEE JOURNAL OF FLEXIBLE ELECTRONICS. He is the Chair of the Italian Section of URSI Commission D Electronics and Photonics and the Co-Founder and the President of the University spin-off RADIO6ENSE that is active in the short-range electromagnetic sensing for Industrial Internet of Things, smart manufacturing, and automotive and digital health. He is listed in the PLOS ranking of Top 1.5% Scientists Worldwide.